FINITE ELEMENT ANALYSIS OF ALUMINA-MILD STEEL WELDED TUBE OF INTERNAL STRESSES

[1]*G.R.KRISHNA PRASAD REDDY,*[2]*A.RAVI KIRAN*
[12]*Assistant Professor*
Department Of Mechanical Engineering
CVRT Engineering college, Tadipatri

ABSTRACT:
In this paper to Evaluation of mechanical and interfacial properties of friction welded alumina-mild steel rods with the use of Al6061 sheet are presented in this work. The bonds were attained through interfacial interlocking and intermetallic phase formation with average bending strengths in the range of 40 to 200 MPa and insignificant hardness change in the parent alumina and mild steel. A preliminary simulation was made to predict the deformation, stress, strain and temperature distribution during the joining operation using a fully coupled thermo-mechanical FE model. The aluminum alloy metal being rubbed was simulated using a phenomenological Johnson-Cook viscoelasticity material model, which suited for materials subjected to large strains, high strain rates and high temperatures. The highest stress, strain and deformation are found to be within the heat affected zone of the weld close to the periphery rubbing surface region and correspond to the highest temperature profiles observed.
Keywords: friction welding, intermetallic, FE model, interface, bending strength

1.0 INTRODUCTION

The friction welding of 6061-T6 aluminum and AISI 1018 steel and suggested that a thin, discontinuous intermetallic layer formed at the bond line was a result of interdiffusion between iron and aluminum. Intermetallic generally result in mechanical degradation of the joint **[1].** The formation of these phases is mainly driven by interdiffusion of the species and is highly dependent on the specific time and temperature history of the welding process. The extended thermal cycles (higher temperatures/longer times) associated with fusion welding processes generally result in the formation of thick intermetallic compound (IMC) layers at the joint interface **[2].** The formation of these layers is generally considered the root cause for property degradation seen with these types of joints. FW can facilitate joint formation at lower temperatures, often at very short times, and is generally associated with reduced formation of these intermetallic phases. For ceramics - metal welding, the intermediate layer apart from thermo-plastic deformations of metal plays a significant role **[3].** It seems that besides adhesion, the diffusion of atoms from the metal layer into the ceramic foundation can cause sealing of a ceramic material with metal. This is confirmed by the results of investigation on linear distribution of elements, carried out by means of electron probe techniques **[4]**. The gradient of aluminum concentration, temperature gradient and stress field are the factors that power the atom migration in metal during the welding process. The predicted the average diffusion coefficient of Al to Alumina ($D = 1.8 \times 10^{-13}$ m^2/s) in friction welded Alumina-Al6061 and stated that the diffusion region occurred in several micro meter's distances.

Scope of the study

To analyse mechanical strengths and interfacial properties in bonded alumina-mild steel rods during the friction welding process where an interlayer Al6061 sheet is used. A preliminary simulation is made to predict the deformation, stress, strain and temperature distribution during the joining operation using a fully coupled thermo-mechanical FE model.

2.0 LITERATURE REVIEW

In recent years, the use of joints between dissimilar metals has considerably increased. In the development of new technologies for the aerospace, medical and automotive industries, these junctures are of high importance, because they allow the systems, components manufactured in mild steel and aluminum to be structurally united Sepe, R.; Armentani **[5]** performed a study in a dissimilar welding butt joint (titanium and aluminum), using a fiber laser welding method. 2D and 3D Gaussian heat source were used to study the thermal analysis of this welding process. The experimental fusion zone of the joint was compared with the numerical one. During the welding cycle, the actual temperature was registered and was validated by the numerical model. To calculate fusion zone's dimension, the 2D model

demonstrated better accuracy than the 3D. Dhinakaran, V.; Siva **[6]** developed a simulation model considering both in-plane and out-of-plane distortions. This model was validated with case study analysis and the results demonstrated good agreement in predicting and diagnosing the in-plane variation. Dhinakaran et al **[7]** performed a finite element analysis to understand multi-layer rotating arc narrow gap MAG welding for medium steel plate. Temperature field was solved and analyzed in multi- layer rotating arc welding based on element birth and death technique. The simulation results were in good agreement with the experimental data, 1.5 mm of difference between them. Residual stress and deformations were calculated based on temperature fields in four welding conditions Derakshshan et al **[8]** performed full 3D simulations in studying the start/stop in partial repair effects. The start and stop events have been simulated in 3D, and comparison, with 2D results, indicate a significant increase in weld residual stresses. These events are harmful to reliability since the extra thermal and mechanical loading increases the stress height, which can influence the crack depth or the initiation of failure by Balran, Y.; Babu **[9]** Finite element model has been developed to predict the temperature fields and residual stress distribution in weldments. A coupled sequentially thermo-mechanical transient analysis was used to carry out with ANSYS 16.0. The temperature dependent properties of base metals are considered during the welding modeling. The heat flow rate during the welding due to conduction, convection and radiation was considered Balakrishnan, J **[10]** In this work we assess the effects that two current technologies, and two candidate technologies for future build programmes, are likely to have on the generation of residual stresses within critical nuclear components. Single-sided welds were manufactured in 30 mm thick plates of SA508 steel, using four welding processes: gas-tungsten arc welding (GTAW), submerged-arc welding (SAW), multi pass NGLW and RPEB welding.

3.0 METHODOLOGY

In the experimental study, rods 10 mm in diameter made of alumina (50 mm length) and mild steel (50 mm length), and Al6061 sheet (0.3 mm, 0.5 mm, 1.0 mm and 1.5 mm) interlayers were used. The connection surfaces of mild steel and alumina were ground to smooth and sharp edges around it. The experimental setup for the FW process is shown in

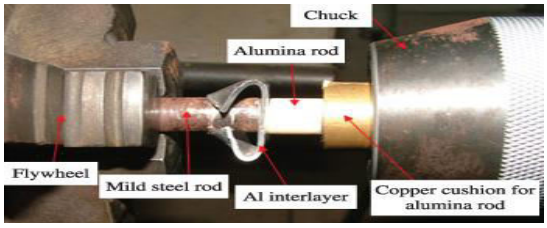

Figure 3.1: Experimental setup

The friction welded sample was sectioned perpendicular to the weld interface and polished. Macrograph and microstructure of the weld interface were obtained using Dino-Lite digital microscope and Field Emission Scanning Electron Microscopy (FESEM) (model VPFESEM SUPRA 35VP) machine respectively. Electron-probe microanalysis (EPMA) was carried out across intermediate layers to determine the variation of element concentration using FESEM. The successfully welded samples at various friction times were also measured for their four-point bending strength using Instron machine (model 8501) and Knoop hardness test.

The friction welding process was done on a continuous drive friction welding machine. The friction welding conditions were 900 rpm rotational speed and 20 MPa axial pressure. The bending strengths and hardness values of the welded samples were determined. The successful joined alumina-mild steel rods are shown

Figure 3.2: Alumina and steel weld joints

The main heat source in FW is generally considered to be the friction between the rotating rod (mild steel)-interlayer (aluminium alloy) sheet surfaces and the un rotating rod (alumina)-interlayer (aluminum alloy) sheet surfaces, and the "cold work" in the plastic deformation of the interlayer. The heat generation from the plastic deformation of the aluminum is considered to some extent in the model with the use of variable friction coefficient and not explicitly accounted for as a heat source. The heat is generated at the interface of the rotating steel rod and the aluminum sheet due to friction and plastic deformation

Boundary and initial conditions

The conduction and convection coefficients on various surfaces play an important role in the determination of the thermal history of the workpiece in friction welding. The initial and boundary conditions considered in this model are based on the actual conditions exhibited in experiment figure shows the various boundary conditions applied on the model.

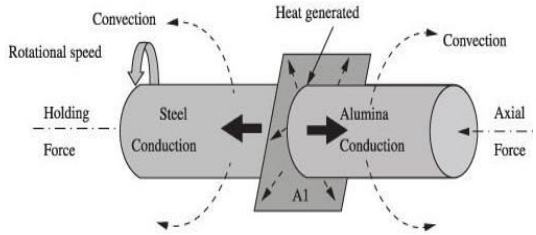

Figure 3.3: Boundary conditions applied weld joints

FEM model

To model the actual physics phenomena of the FW process is rather complicated. Therefore, several simplifying assumptions have been made. The assumptions made when defining the loads and boundary conditions for the simulation are

Perfect elastic-plastic behaviour of the work pieces material was assumed also to reduce computer time requirements;

- The interlayer and rods were assumed to experience frictional contact described by Coulomb's frictional law with temperature dependent friction coefficient, μ;
- The friction coefficient, μ below material melting point were assumed to be zero following the tendency from the experimental chart[13];
- The radiation heat loss was neglected as it was considerably less compared to the conduction and convection losses.

The alumina and steel rods were modelled in the computational domain of 20 mm length and 10 mm diameter each. The aluminum alloy sheet was modeled in the computational domain of 1.42 mm thickness and 12 mm diameter. The alumina and steel rods were modelled using 3D solid (continuum) elements as deformable rigid constrained. The aluminum sheet was modelled as a solid and deformable element. The attachment of aluminum sheet to the steel rod end surfaces was considered to be perfectly.

In this analysis, a uniform connection was assumed. The plasticized zone was the heat generated and affected area where the aluminum turned to be softened due to severe friction. In this zone the material model of Johnson-Cook and adaptive meshing were incorporated during simulation to enable the occurrence of the aluminum deformation. Coulomb friction law has been selected for the modelling of the workpieces interface contact. Heat transfer is allowed on the components contact area. The boundary conditions, contact conductance in the heat sink, the convection on the external surfaces and sliding surfaces on contact surfaces are applied on the assembled components of aluminum, steel and alumina. Initial temperatures for all components were assumed at 29 °C. The aluminum alloy edge was constrained to move axially.

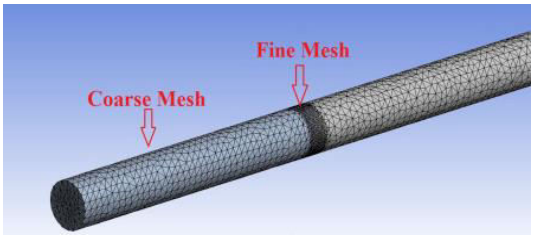

Figure 3.4: Fem model friction weld process

The FE analysis was conducted by prescribing steel rod rotation and followed by displacement of the alumina rod with appropriate boundary conditions. The friction welding simulation was prescribed in three-time steps, based on an actual experimental setup. In the first step, the steel rod was rotated at angular velocity of 94.3 rad/s. Then in the second step, the alumina rod was axially displaced with a rate of 20.8 m/s to the aluminum alloy sheet. Lastly in the third step, after the rubbed interface reached appropriate welding temperature, the rotating steel rod was stopped for cooling stage.

4.0 RESULTS AND DISCUSSION

The reliability of friction-welded ceramic-metal joint with the use of interlayer depends upon the bending strength of the joint which is usually related to interlayer thickness and friction time of the joint. In this section, the relationships between the interlayer thickness, friction time and bending strength were investigated. Here, the bending strength was the average value of 4 joints welded under the same welding conditions. Most of the tested samples fractured in the alumina rod part indicating that the joint is stronger than the brittle alumina body. Most of the tested samples fractured in the alumina rod part as shown in figure This indicates that the joint is stronger than the brittle alumina body.

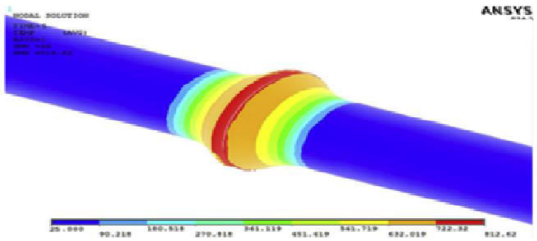

Figure 4.1: Simulated thermal distribution-1

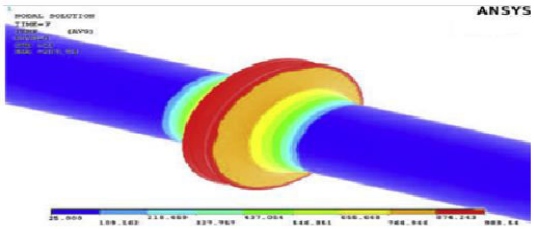

Figure 4.2: Simulated thermal distribution-2

Figure 4.3; After bending test samples

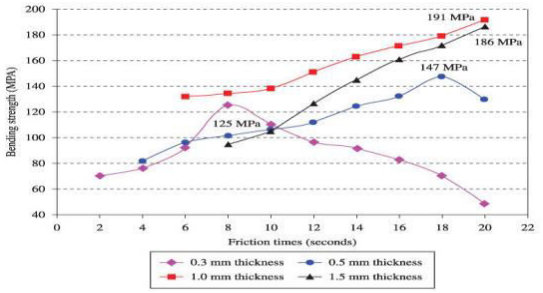

Figure 4.4: Inter layer thickness friction time bending strength of the joints

shows the above figure relationship between the interlayer thickness, friction time and bending strength of the joints. The use of interlayers1.0 mm and 1.5 mm in thickness revealed that the bending strength increased almost proportionally with the increase in friction time ranging from 60 to 200 MPa, except for joints with 0.3 mm and 0.5 mm interlayers.

HARDNESS PROPERTY AT DIFFERENT POINT NEAR THE BONDLINE:

The hardness profile near the bondline of the alumina-mild steel joint is shown in figure the hardness profile in the alumina part exhibited insignificant change and remained constant like before the friction process occurs, i.e. within the range of 1300-1700 KHN. Because alumina has inert, hard and brittle properties, only aluminum atom diffusion occurs at the contact surface during the friction process. On the other hand, the hardness value for the mild steel part slightly increased towards the joint (reaching 200 KHN). This resulted from the effects of the formation of the narrow brittle intermetallic phase at the mild steel - aluminum interface, as discussed in the interfacial microstructure characterization

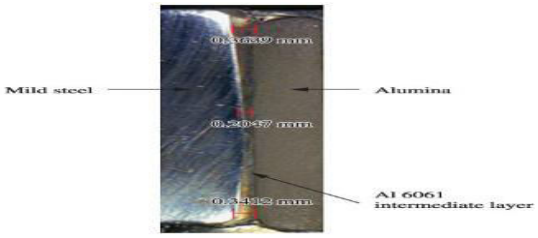

Figure 4.5: Weld cross section

Temperature distribution

Since the heat flux is generated at the rod/interlayer interfaces, the heat flows through the intermediate layer into the alumina and steel rods creating a thermal profile. The simulation is stopped when the maximum aluminum temperature reached reasonable value below its melting point as discussed earlier in section It is observed that the heating temperature of the aluminum-alumina is in the range of 400-450 °C to obtain the joint as has been claimed in the past from other author the variation of the temperature in the cross-section of the joint and the rubbing surface of the interlayer throughout the simulation run for the constant steel rod rotation speed of 900 rpm. Increase rapidly in axial load increases the surface heat flux in the deformed aluminum, particularly in the region adjacent to the rods periphery. This leads to higher temperatures which are observed in the simulation results. As it can be observed a maximum temperature of 449.4 °C has been achieved in the early deformed aluminum sheet at 0.0001 seconds.

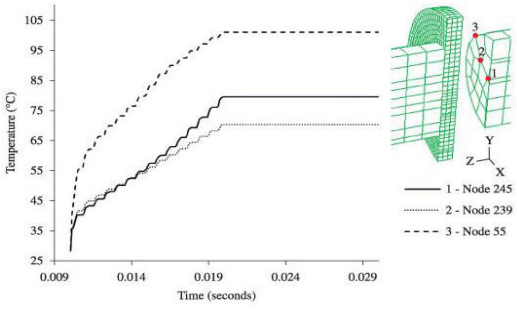

Figure 4.6: Weld joints entire process period

The temperature increases rapidly from room temperature up to almost 130 °C. Due to friction mechanism, the temperature then rises and fluctuates further until 150 °C before slowly decreases when the steel rod rotation is stopped. Following the same trend, both inner nodes 245 and 250 show overlap curves. During the FW

process, temperature at the two nodes increase rapidly up to 110 °C and steadily rises up to 150 °C before slowly decreases after the FW stopped.

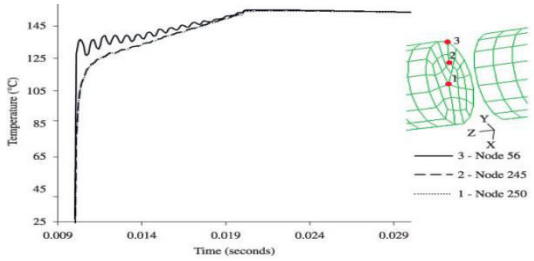

Figure 4.7: Temperature at friction steel - Alumina function of time during period

STRAIN AND STRESS DISTRIBUTION

Figure shows the Von Mises stress and equivalent plastic strain contour maps of the interlayer rubbing surface at friction welding time of 0.0053 seconds. As it can be observed, the maximum plastic strain reaches the value of 6, and is generated where the largest plastic strains take place in the material close to the rod periphery, since the material is subjected to intense deformations due to the rod's translational and rotational motion. This issue matches with the maximum deformed interlayer temperature found at the same zone.

Regarding the Von Mises stress distribution shown in figure it is important to keep in mind that, in the model, the yield stress was given as a function of temperature and the values ranged from around 510 MPa at room temperature to less than 21 MPa at temperatures greater than 300 °C. As can be observed, the material close to the contacted rod experienced yielding and the maximum stress appears in the interlayer contacted surface, near the periphery zone of the contacted diameter.

There are several key parameters in the model that have a significant impact in the simulation results: the coefficient of friction between the rod and the interlayer material, the limiting shear stress that controls the stick/slip condition between contacting surfaces and the distribution of frictional heat between the rod and the interlayer sheet. Ideally, carefully designed experiments should be conducted to determine the value of those parameters.

CONCLUSIONS

This work demonstrated the creation of bond through interfacial interlocking and intermetallic phase formation with average joint bending strengths in the range of 40 to 200 MPa depending on friction time and interlayer thickness. Thinner interlayers could not maintain the increment of strength due to large material depletion. The strength was degraded by the existence of incomplete joint observed at the interface when a thinner interlayer was used. The hardness value for the mild steel part slightly increased toward the joint because of the formation of aluminium-mild steel intermetallic phase but this was not happening in the alumina part. The joint was created through the mechanical interlocking of aluminium-alumina interface and the formation of intermetallic phase across aluminium-mild steel interface. The fully coupled thermal-mechanical FE model, the peak temperature, the fields of temperature, deformation, stresses and strains are successfully analysed where maximum values are mostly predicted to be around the periphery of the rubbing surface. The combined features of this approach allow the coupled thermo-elasto-plastic response to be obtained, which clearly shows the extent of the thermo mechanically affected zone and the temperature profile immediately after the operation is completed. While the predicted overall deformation shapes are reasonable considering the assumptions made, further refinements are needed to obtain flash during the operation. Also, more realistic representation of the temperature dependent elastoplastic material behavior would be expected to decrease the predicted temperatures to more realistic values. Even though the FE model proposed in this study cannot replace a more accurate analysis, it does provide guidance in weld parameter development and enhances understanding of the friction welding process, thus reducing costly and time-consuming experimental approaches.

REFERENCE:

1. W. R. Longhurst, A. M. Strauss, G. E. Cook, and P. A. Fleming, “Torque control of friction stir welding for manufacturing and automation,” *International Journal of Advanced Manufacturing Technology*, vol. 51, no. 9-12, pp. 905–913, 2010.
2. T. P. Suresh and S. Sampathkumar, “Role of axial thrust in the formation of microstructure and fracture surface of the weld zone in friction stir welded AA6063 aluminium alloy,” *International Journal of Materials Research*, vol. 105, no. 1, pp. 50–57, 2014
3. F. Lambiase, V. Grossi, and A. Paoletti, “Effect of tilt angle in FSW of polycarbonate sheets in butt configuration,” *International Journal of Advanced Manufacturing*

Technology, vol. 107, no. 1-2, pp. 489–501, 2020.

4. J. S. Sashank, P. Sampath, P. S. Krishna, R. Sagar, S. Venukumar, and S. Muthukumaran, "Effects of friction stir welding on microstructure and mechanical properties of 6063 aluminium alloy," *Materials Today Proceedings*, vol. 5, no. 2, pp. 8348–8353, 2018.
5. Sepe, R.; Armentani, E.; Lamanna, G.; Caputo, F. Evaluation by FEM of the influence of the preheating and post-heating treatments on residual stresses in welding. Key Eng. Mater. 2015, 627, 93–96
6. Dhinakaran, V.; Siva Shanmugam, N.; Sankaranarayanasamy, K. Experimental investigation and numerical simulation of weld bead geometry and temperature distribution during plasma arc welding of thin Ti-6Al-4V sheets. J. Strain Anal. Eng. Des. 2017, 52, 30–44.
7. Rathod, D.; Francis, J.; Vasileiou, A.; Roy, M.; English, P.; Balakrishnan, J.; Smith, M.; Irvine, N. Residual stresses in arc and electron-beam welds in 130mm thick SA508 steel: Part 1—Manufacture. Int. J. Press. Vessel. Pip. 2019, 172, 313–328.
8. Derakshshan, D.; Yazdian, N.; Craft, B.; Smith, S.; Kovacevic, R. Numerical simulation and experimental validation of residual stress and welding distortion induced by laser-based welding processes of thin structural steel plates in butt joint configuration. Opt. Laser Technol. 2018, 104, 170–182.
9. Balran, Y.; Babu, B.; Vardhan, T.; Ramana, G.; Chakradhar, G. Residual stress analysis of dissimilar tungsten inert gas weldments of AISI 304 and Monel 400 by numerical simulation and experimentation. Mater. Today Proc. 2019.
10. Balakrishnan, J.; Vasileiou, A.; Francis, J.; Smith, M.; Roy, M.; Callaghan, M.; Irvine, N. Residual stress distributions in arc, laser and electron-beam welds in 30 mm thick SA508 steel: A cross-process comparison. Int. J. Press. Vessel. Pip. 2018, 162, 59–70